

# Large-scale extreme rainfall producing synoptic systems of the Indian summer monsoon

Akshaya C. Nikumbh<sup>1,2,3</sup>, Arindam Chakraborty<sup>1,2</sup>, G.S. Bhat<sup>1,2</sup>, Dargan M.  
W. Frierson<sup>3</sup>

<sup>1</sup>Centre for Atmospheric and Oceanic Sciences, Indian Institute of Science, Bangalore, 560012, India.

<sup>2</sup>Divecha Centre for Climate Change, Indian Institute of Science, Bangalore, 560012, India.

<sup>3</sup>Dept. of Atmospheric Sciences, University of Washington, Seattle, 98195, USA.

## Key Points:

- A mechanism for large-scale extreme rainfall events of central India is proposed.
- Large-scale extreme rainfall events occur when monsoon low pressure systems are assisted by secondary cyclonic vortices.
- The interaction of two cyclonic vortices form conditions favourable for long-lived, organized, and slow moving convective systems.

---

Corresponding author: Akshaya C. Nikumbh, [nikumbh@iisc.ac.in](mailto:nikumbh@iisc.ac.in)

## Abstract

In recent years India has been increasingly experiencing widespread floods induced by large-scale Extreme Rainfall Events (LEREs). LEREs are mainly associated with monsoon Low-Pressure Systems (LPS). The forecast of these high-flood-potential events, however, has remained challenging. Here, we compare LPSs of the summer monsoon that led to LEREs (LPS-Lg) and strong LPSs that did not result in LEREs (LPS-noLg) over central India for the period 1979-2012. We show that having a strong LPS is not a sufficient condition to produce LEREs, and the LPS-Lg are accompanied by Secondary Cyclonic Vortices (SCVs). The simultaneous existence of an LPS and an SCV creates a giant mid-tropospheric vortex. SCVs enhance dynamic lifting, static instability, and moisture transport from the Arabian Sea that precondition the atmosphere for deep convection. SCVs also slow down the propagation of LPSs. We show that the interaction of synoptic-scale systems can lead to LEREs even if individual systems are not strong enough.

## Plain Language Summary

Over the past two decades, India has endured many widespread floods caused by large-scale heavy rainfall events during the monsoon season that resulted in huge losses to life and property. The large-scale heavy rainfall events, though rare, have become more frequent recently. We show that these events occur when multiple monsoon low pressure systems are present at the same time. While the individual systems themselves need not be very strong, their simultaneous presence makes the environment conducive for sustained and organized deep convection, leading to large-scale heavy rainfall events over central India.

## 1 Introduction

Understanding the physical processes that lead to extreme rainfall events (EREs) is a challenging multiscale problem that has received wide attention in the literature. The literature on EREs includes aspects like flash floods (Maddox et al., 1978, 1979; Bosart & Sanders, 1981), convective systems (Doswell III et al., 1996; Schumacher & Johnson, 2005), the observed trends (B. N. Goswami et al., 2006; Rajeevan et al., 2008; Karmakar et al., 2017; Nikumbh et al., 2019), and their future projections (Trenberth, 1999; Emori & Brown, 2005; Muller et al., 2011; O’Gorman, 2015). A multitude of extreme precipitation events, however, remained unpredicted (Coumou & Rahmstorf, 2012). Predicting the location and intensity of extreme precipitation, and avoiding false alarms continue to be major challenges in weather forecasting. Though EREs have different features based on their time and location, there are certain common characteristics that can be used for their forecasting. The ingredients for extreme precipitation include moist ascent, static instability, dynamic lifting and moisture supply (Doswell III et al., 1996). These ingredients are often brought together in the presence of synoptic systems and hence EREs are often associated with synoptic systems.

During the Indian summer monsoon season, a large part of kinetic energy at mid levels is contributed by synoptic systems such as Low Pressure Systems (LPSs) and Mid-Tropospheric Cyclones (MTCs) that form over the surrounding ocean and the Indian subcontinent (Krishnamurti & Hawkins, 1970). LPSs form most frequently over the Bay of Bengal (BoB) and move north-westward over the Indian subcontinent (Sikka, 1978; Godbole, 1977). They contribute around half of the rainfall over the core monsoon zone (Hunt & Fletcher, 2019; Sikka, 1977) and often lead to heavy rainfall events over central India (Ajayamohan et al., 2010). The southwestern sector of LPSs is known to receive heavy rainfall, often exceeding  $300 \text{ mm day}^{-1}$  (Godbole, 1977; Krishnamurthy & Ajayamohan, 2010). In the past two decades, India has experienced many devastating floods triggered by extreme rainfall viz., the Kerala flood of August 2018 (Baisya & Pattnaik, 2019), Chennai flood of Dec 2015 (Phadtare, 2018; Chakraborty, 2016), Uttarakhand flood of June 2013 (Houze Jr et al., 2017), Leh flood of June 2010 (Rasmussen & Houze Jr, 2012), and Mumbai

flood of July 2005 (Kumar et al., 2008). Though each individual event had unique features, the common thread in all events was the presence of an LPS. In every season around 15 to 18 LPSs are observed (Figure 1a) and almost two-third produce at least one ERE over central India and remaining 33% do not give extreme rainfall. A comprehensive understanding of the conditions that stimulate LPSs to produce EREs is missing. To address the problem of false alarms it is important to understand the conditions under which LPSs are more likely to give rainfall extremes.

EREs over the west coast of India are often associated with synoptic systems such as MTCs, off-shore troughs, and vortices (Francis & Gadgil, 2006; Pradhan et al., 2015; Carr, 1977). An active offshore trough (Wang, 2006) and mesoscale vortices (George, 1956) often lead to heavy rainfall reaching over  $300 \text{ mm day}^{-1}$  to  $500 \text{ mm day}^{-1}$  near the west coast (Wang, 2006). Past studies have extensively examined the influence of MTCs and offshore trough/vortices on heavy rainfall events over the western states (Miller & Keshavamurthy, 1968; Francis & Gadgil, 2006; Pradhan et al., 2015; Carr, 1977). However, the possibility of synoptic systems of the west coast influencing heavy rainfall events further eastward, over central or eastern Indian states has not been explored yet.

It has been observed that the Large-scale Extreme Rainfall Events (LEREs, area  $\geq 70 \times 10^3 \text{ km}^2$ ) over central India are increasing significantly (Nikumbh et al., 2019). The LEREs are of a great concern as they are more likely to cause widespread flooding compared to small-scale scattered events. For example, the recent flood over India in the first week of August 2019 (Carlowicz, 2019), Kerala flood of mid-August 2018 (Baisya & Pattnaik, 2019), Gujarat flood of July 2017 (Thiruppugazh, 2019) were caused by the widespread extreme rainfall events that spanned over the entire state and resulted in hundreds of deaths. This underscores the urgency of improving an understanding of the physical process that lead to LEREs. The LEREs of the Indian summer monsoon are predominantly associated with monsoon LPSs (Nikumbh et al., 2019). During the monsoon season there is a high chance (probability=0.66) of getting an ERE over central India given an LPS, however, probability of getting an LERE is extremely rare (probability=0.04) (Figure 1a). This poses some interesting questions: why do so few LPSs result in LEREs? Are LEREs associated with some of the strongest and rare LPSs? In this study we pursue these questions by comparing characteristics of LPSs and meteorological conditions that lead to LEREs (LPS-Lg) and strong LPSs (intensity  $\geq 2$ ) that did not result in LEREs (LPS-noLg).

## 2 Datasets and methods

We use the daily  $1^\circ \times 1^\circ$  gridded rainfall dataset prepared by the India Meteorological Department (IMD) (Rajeevan et al., 2006) for the monsoon months (June to September) of the period 1979 to 2012. The EREs are defined following the same procedure as in Nikumbh et al. (2019). The 99.5<sup>th</sup> threshold is used to define extreme rainfall at each grid and then the neighbouring grids with simultaneous extreme precipitation are combined using the connected component labelling algorithm (Falcão et al., 2004). The EREs that span over an area more than five  $1^\circ \times 1^\circ$  grids (area  $\geq 70 \times 10^3 \text{ km}^2$ ) are defined as LEREs. Then we iteratively check the consecutive days of EREs to find if there is an overlap over at least one grid cell of the location of EREs. If an overlap in the locations of EREs exist for the consecutive days, only the first day of the largest EREs is considered for the calculation. This makes sure that the same event is not counted again. Over the Indian subcontinent, the LEREs occur mainly between  $15^\circ$  to  $25^\circ\text{N}$  (Nikumbh et al., 2019) and we select this region ( $15^\circ$ - $25^\circ\text{N}$ ,  $65^\circ$ - $85^\circ\text{E}$ ) as our study area (boundaries shown in Figure 1b). Over the study region 24 such LEREs were observed from 1979 to 2012.

The dataset by Hurley and Boos (2015) is used for LPSs. This dataset identifies LPSs using ERA-Interim 850 hPa relative vorticity. They applied an automated tracking algorithm (Hodges, 1995, 1999) on a 6-hourly 850 hPa relative vorticity field. The tracking algorithm is based on the optimization of the cost function for motion (Hodges, 1999). It

is used to identify relative vorticity maxima (or minima in the southern hemisphere) and to track its path. Only those vortices are considered whose maxima (or minima) exceeds a magnitude of  $0.5 \times 10^{-5} \text{ s}^{-1}$ . Additional filtering criteria includes that the LPS should last for two or more days and should have at least one point of the track is in the monsoon region. They use additional criteria of the mean sea-level pressure anomaly and surface wind speed (10 m) to define the intensity of LPS. The intensities 1 and 2 correspond to monsoon lows (pressure anomaly  $\geq 2 \text{ hPa}$ ) and depressions (pressure anomaly between 4 to 10 hPa and wind speed between  $8.5 \frac{\text{m}}{\text{s}}$  and  $13.5 \frac{\text{m}}{\text{s}}$ ) respectively. Intensity 3 indicates deep depression and above (pressure anomaly  $\geq 10 \text{ hPa}$  and wind speed  $\geq 13.5 \frac{\text{m}}{\text{s}}$ ). The presence of LPSs is checked for each LERE within the domain of  $10^\circ\text{-}30^\circ\text{N}$ ,  $65^\circ\text{-}85^\circ\text{E}$  (LPS domain). Out of 24 LEREs, 22 had the presence of LPSs. We compare these 22 LPSs that led to LEREs (LPS-Lg) and 132 strong LPSs (intensity  $\geq 2$ ) that passed through the LPS domain but did not cause LEREs (LPS-noLg). For the meteorological variables, the daily data from the ECMWF interim reanalysis (ERA-Interim; (Dee et al., 2011)) is used, at the spatial resolution of  $1^\circ \times 1^\circ$ .

Secondary Cyclonic Vortices (SCVs) to the west of LPSs are confirmed by relative vorticity maps (Figure S1, Figure S2). The type of weather systems associated with SCVs are verified using the IMD weather reports. The SCVs are reported either as cyclonic circulation or monsoon lows in the IMD weather report (details in supplementary information).

### 3 Results and discussions

#### 3.1 LPSs and extreme rainfall events

The average number of LPSs observed over the study region per season is 15. Around 66% of LPSs during the study period were associated with at least one ERE over the study region. Though the number of LPSs that results in EREs varies from year to year (Figure 1a), there is not a single year when LPSs of the monsoon season did not cause any ERE over central India. This supports the idea of a strong association between EREs over central India and LPSs. On the other hand, there are 2 to 5 LPSs in a season that pass through central India without causing any EREs, thus underscore the uncertainty tied to this association between LPSs and EREs.

The relative vorticity distribution (Figure S3) for the two types of LPSs show that the LPS-Lg have a higher median vorticity ( $7 \times 10^{-5} \text{ s}^{-1}$ ) than LPS-noLg ( $6 \times 10^{-5} \text{ s}^{-1}$ ). However, there are many LPSs in LPS-noLg that had higher relative vorticity than LPS-Lg. During the study period, out of the 9 strongest LPSs (with intensity  $\geq 3$ ) only 3 led to LEREs. On the other hand, 82% of LEREs were associated with LPSs with intensity  $\geq 2$ . This suggests that the LPSs that lead to the LEREs tend to be stronger, but their strength is not a sufficient condition to get LEREs.

#### 3.2 Large-scale extreme rainfall events

The LEREs show a peculiar geographical preference. They occur mainly over the zonal belt in between the frequent locations of synoptic systems of the east and west coast (Figure 1b). The mean seasonal climatology of geopotential height at mid-levels captures these two frequent locations of synoptic systems that have centers around  $\sim 84^\circ\text{E}$  and  $\sim 72^\circ\text{E}$  (Karmakar et al., 2015). As LPSs of the east coast are more frequent, the eastern location is better defined with sharper gradients than the west. Note that both of these centers are present around the same latitudinal belt ( $18^\circ - 20^\circ\text{N}$ ) with the west center being slightly southward ( $\sim 18^\circ\text{N}$ ). Consequently, there are two locations where the LEREs occur most frequently, one near the east coast ( $\sim 80^\circ\text{E}$ ) and the other near the west coast ( $\sim 76^\circ\text{E}$ ). The climatological surface monsoon trough (Y. Rao, 1976) and low-level jet (LLJ, shown in Figure S4) (Findlater, 1969; Joseph & Sijikumar, 2004) lie on the northern and southern side of LEREs, respectively.

The LEREs occur in the southwestern sector of LPSs (Nikumbh et al., 2019). We observe that the LPS-Lg are accompanied by SCVs on their western flank (Figure S1). Of all the SCVs that occurred with LPS-Lg, 57% were identified as cyclonic circulation and 24% as monsoon lows in the IMD weather reports. The cyclonic circulation includes the lower- or mid-tropospheric systems, and the monsoon lows refers to the lows, depressions and cyclonic storms. 19% of SCVs were not identified as weather systems by the IMD, however, the presence of a vortex (vorticity  $\geq 2 \times 10^{-5} \text{ s}^{-1}$  at 500 hPa and 850 hPa) has been manually verified using the vorticity map (Figure S1, Figure S2).

There are two frequent genesis regions for LPS-Lg over the BoB, one at  $20^\circ\text{N}$  and the other at  $15^\circ\text{N}$  (Figure 1c). The LPS-Lg tracks are southward compared to LPS-noLg. The LPS-Lg show a westward extension of LPSs tracks. The LPS-noLg have a shorter path and their genesis locations are mainly observed in the north BoB ( $\sim 20^\circ\text{N}$ ) (Figure 1d). As the LPSs on the southern side are more likely to encounter the effect of synoptic systems of the west coast (Figure 1c), the genesis location and track density of LPS-Lg paths show a peak on the southern side ( $\sim 15^\circ\text{N}$ ). The westward extension of the path of LPS-Lg possibly indicates a long lifetime of LPS-Lg. In the next sections, we examine how the interaction between LPSs and SCVs lead to LEREs.

### 3.3 Mid-tropospheric vortex, dynamic lifting and organized convergence

Two days before the LEREs, the presence of both an LPS over the BoB and an SCV over the west coast is evident at 500 hPa (Figure 2a). The LPS continues to move westward and the circulations associated with both vortices merge a day before the event. This leads to the formation of a giant mid-tropospheric cyclonic vortex (MCV) over central India. An MCV is often observed in long-lived mesoscale convective systems (MCSs) (Bartels & Maddox, 1991; Fritsch et al., 1994; Bartels et al., 1997). A vorticity budget analysis suggests that it forms by advection of vorticity from the environment and generation of vorticity by MCSs themselves (Knievel & Johnson, 2002, 2003). MCSs that develop a stratiform region perturb the vertical temperature gradient and tends to concentrate positive potential vorticity at midlevel, which manifests as a midlevel vortex (Raymond & Jiang, 1990). The MCV in turn promotes new convection and extends the lifetime of MCSs (Fritsch et al., 1994; Raymond & Jiang, 1990). MCVs also help in organizing the deep convection (Schumacher & Johnson, 2009). The mid-level vortex generated by interaction of LPS and SCV thus could help in forming long-lived organized convection conducive for widespread extreme rainfall.

Strong ascent associated with the LPS and a comparatively weaker SCV ascent are apparent in the vertical structure of pressure velocity (omega) (Figure 2b). Rising motion is observed on the west and sinking motion on the east of cyclonic vortices, as observed in earlier studies (Krishnamurti & Hawkins, 1970; Sikka, 1978). Both SCV and LPS exist in an easterly sheared environment owing to reversal of the meridional temperature gradient. The interaction of these vortices with easterly shear produces the maximum ascent on the western side (K. Rao & Rajamani, 1970; Sanders, 1984). This can be simply shown by using an approximate form of the quasi-geostrophic equation (Sutcliffe, 1947; Trenberth, 1978; Boos et al., 2015)

$$\Delta w \sim f_o \frac{\partial u_g}{\partial p} \cdot \nabla (2\xi_g + f) \quad (1)$$

Where,  $\Delta$ -Laplacian operator,  $w$ -pressure velocity,  $f$  and  $f_o$  are the Coriolis parameter and the mean Coriolis parameter, respectively, and  $u_g$  and  $\xi_g$  are the geostrophic wind and its relative vorticity, respectively. The right-hand side of Eq. (1) gives the dynamic generation of rising motion downshear of a vorticity maximum. The temperature distribution and warm advection also contribute to ascent on the western side of these systems (Krishnamurti & Hawkins, 1970; Adames & Ming, 2018a, 2018b).

The ascent of the SCV is horizontally narrow, vertically not that deep and stays almost at the same location (from day-2 to day-0). The westward moving LPS has a larger

spatial extent and is deeper too. The orographic flow (leeward subsidence) associated with the Western Ghats is possibly preventing the low level connection between the two (Figure 2b). There is also a location of ascent at the junction of LPS and SCV, resulting from the convergence at the meeting point of two systems. At day-0, the ascents merge and form a spatially large ascending region. It has been observed that the long-lived cloud systems are preferentially triggered on the western flank of LPSs, where a steep gradient of low level vorticity and temperature is present (Phadtare & Bhat, 2019). The gradients in vorticity and temperature help in setting up the rising motion (e.g., using QG omega equation) that results in forming a favourable region for long-lived cloud systems on the western flank of LPSs. The large long-lived clouds systems occur on the western flank of LPSs mainly in the band of  $15^\circ - 25^\circ$  N (Figure 11 of Phadtare and Bhat (2019)), which coincides with the location of LEREs of our study. It should also be noted that the adiabatic lifting is not sufficient to explain the deep convective systems on the western flank of LPSs (Adames & Ming, 2018b, 2018a; Boos et al., 2015) and other processes that include moist thermodynamics also add ascent. The moist thermodynamic processes are explored in the section 3.4.

Two days prior to the event, a low-level convergence zone forms on the western side of LPSs, and the north eastern side of SCV (Figure 2c). A day before the event two convergence zone strengthen as the LPS moves westward. On the day of the event both of them merge and form a large-scale organized convergence zone that has northwest-southeast orientation. This convergence zone could in turn support the organized convective systems, leading to widespread EREs. Only the southern part of this convergence zone experiences the LEREs.

### 3.4 Thermodynamic instability and moisture supply

The presence of an SCV provides moist thermodynamic instabilities that play a major role in enhancing the rainfall intensity. Figure 3a shows the vertical cross section of dry static stability, namely, Brunt Vaisala frequency ( $N = \frac{g}{\theta} \frac{d\theta}{dz}$ ). Two days before the event, centers of static instabilities exist at midlevel over central India that are generated by convective heating associated with SCV and LPS. These instabilities merge a day before the event and the anomalies associated with the LPSs intensify even at lower levels. On the day of the event, these instabilities intensify throughout the column up to 250 hPa over central India forming a favourable environment for deep convection.

To examine the effects of moisture, we compare the vertical profiles of potential temperature ( $\theta$ ) and equivalent potential temperature ( $\theta_e$ ) (Figure S5). The moisture supply by the LLJ at low levels is evident since day-2 and it peaks on the day of the event. At day-2, the vertical profiles of  $\theta$  and  $\theta_e$  are similar at upper levels, indicating that moisture effects are small there. At day -1, the  $\theta_e$  deviates slightly from that of  $\theta$  at mid-levels as the moisture flux increases. On the day of the event,  $\theta$  and  $\theta_e$  profiles substantially deviate, indicating a strong moistening throughout the column. Moisture plays an important role in the growth and sustenance of LPSs (Adames & Ming, 2018a). Using a linear framework, Adames and Ming (2018b) studied the relative importance of dry and moist processes in growth and propagation of LPSs. They found that moist processes play a major role in the growth of LPSs. It should be noted that their analysis does not consider the strong background flow and vertical shear that occur during the monsoon. However, it is useful to infer that LPSs could grow just by moist processes (moisture and temperature advection and high humidity) and even without barotropic or baroclinic instabilities. The moisture supply at midlevels has been shown to enhance the vertical development in tropical convection (Bretherton et al., 2004; Holloway & Neelin, 2009). Free tropospheric moisture plays a significant role in relation between column water vapor and the transition to sustained deep convection in the tropics (Holloway & Neelin, 2009). High moisture in the free atmosphere results in higher plume buoyancies and forms conditions favorable for deep convection. The SCVs provide

deep inflow of moisture flux, which helps in sustaining convection in the southwestern sector of LPSs.

The moisture budget can be analysed by moisture transport and convergence. The column integrated moisture transport (MT) is given by,

$$MT = \frac{1}{g} \int_{P_a}^{P_s} q \mathbf{V} dp \quad (2)$$

Where,  $P_s$  and  $P_a$  are surface and top of atmosphere pressure respectively,  $g$ - gravitational acceleration,  $q$ -specific humidity,  $\mathbf{V}$ -horizontal velocity. The vertical integral of moisture flux divergence (VMFD) is obtained by taking time-integral of the horizontal divergence of equation 2. In this study, we use the VMFD output from ERA-Interim, which was calculated by the reanalysis model.

The Figure 3b-c show the VMFD (shading) and MT (vectors) for LPS-Lg and LPS-noLg. In case of LPS-Lg, three main locations of moisture convergence are observed. One is to the southwest of the SCV, while the second is on the western side of the LPS and the third is to the north of LPSs center. The moisture convergence on the southwest of SCV results from the interaction of an SCV with the moisture flux by LLJ. The region of moisture convergence in the western sector of LPSs results from interaction of LPSs circulation with LLJ. Note that the westerly circulation on the southern flank of SCV enhances the strength of LLJ and in turn the moisture transport from the Arabian Sea. The eastern center forms by easterly moisture flux by the northern branch of LPSs. Since the moisture supply is mainly in the southern part of the organized convergence zone (Figure 2c), it experiences LEREs, while the northern part of convergence zone misses them (Figure S6). In case of LPS-noLg, the west coast moisture convergence zone is absent and the supply of moisture by both the Arabian Sea and the BoB is less compared to LEREs. The above analysis reveals that the moisture transport from the Arabian Sea to central India increases in the presence of an SCV.

### 3.5 Propagation speed of LPSs

The average propagation speed of LPSs observed during the study period is  $5 \text{ m s}^{-1}$ . In earlier studies, the propagation speed of MDs is reported as  $5^\circ \text{ longitude day}^{-1}$ , i.e.  $6 \text{ m s}^{-1}$  (Krishnamurti et al., 1975). From the distribution of velocity, it is clear that LPS-Lg tend to be slightly slower than the LPS-noLg (Figure S7). Around 67% of LPS-Lg have velocities lower than the average velocity ( $< 5 \text{ m s}^{-1}$ ) along their track. The CDFs of velocities of LPS-Lg and LPS-noLg differ significantly using the KS test ( $p\text{-value} < 0.06$ ). The speed of convective system affects the rainfall duration and in turn the accumulation of rainfall over the location (Doswell III et al., 1996). It is often observed that slower convective systems are more likely to give extreme precipitation (Maddox et al., 1978; Doswell III et al., 1996; Schumacher & Johnson, 2009). The presence of the SCV hinders the westward propagation of LPS, which results in increased accumulation of rainfall at the same place.

## 4 Summary

This analysis reveals that it is not only the intensity of LPSs but also the presence of SCV that determines whether LPSs could lead to LEREs. Over India, the latitudinal belt of  $15^\circ - 25^\circ \text{ N}$  is the most favourable zone for the LEREs to occur. This region has frequent occurrences of synoptic systems on the western and eastern sides of mainland India. It is also accompanied by the LLJ and climatological monsoon trough on the southern and northern flanks respectively. This unique meteorological setting forms a favourable environment for LEREs. The simultaneous presence of an SCV helps an LPS by the following means to give an LERE (Figure 4).

**1. Mid-tropospheric vortex:** The interaction of the SCV and LPS circulation form a mid-tropospheric vortex, which is known to enhance the lifetime of MCSs and organize the convection.

**2. Dynamic lifting:** The presence of an SCV increases the area of dynamic lifting on the western flank of the LPSs and leads to widespread ascent at mid levels.

**3. Static instability:** Convection associated with the SCV provides additional static instability that could enhance the intensity of these events.

**4. Moisture supply:** The SCV enhances the deep layer moisture supply from the Arabian Sea that helps in sustaining deep convection.

**5. Organization at low-level:** Large-scale low level organized convergence forms in the region between the SCV and LPS.

**6. LPS translation speed:** The presence of the SCV on the western flank of the LPS slows down its westward propagation speed, which results in more accumulation of rainfall at the same location.

These factors provide favourable conditions to form long-lived, organized, slow moving convective systems that lead to LEREs. Our analysis could prove useful to understand the rising trend of precipitation extremes over central India, which has remained a puzzle. It gives a hint for how it is possible to get an increasing trend of LEREs in spite of an observed decreasing trend in stronger LPSs (Dash et al., 2004; Vishnu et al., 2016). We give an example of how synoptic systems could remotely influence EREs. For example, we show that synoptic systems of the west coast of India (MTCs or LPSs) can influence rainfall extremes over central and eastern states of India. Previous studies have noted the temporal and spatial clustering of synoptic activity during the active phase of monsoon (B. Goswami et al., 2003; Murakami et al., 1984). So, the predictability of LEREs could be pursued further by exploring the modulation of synoptic systems by monsoon intraseasonal oscillations, tropical waves, and Madden Julian oscillation. We recommend that a combined index that considers the simultaneous presence of multiple synoptic systems would prove more useful in the forecasting of widespread heavy rainfall events.

## Acknowledgement

AC and GSB acknowledge funding from the DST, MoES and MoEF, Government of India. DMWF is supported by NSF grant AGS-1665247. ACN acknowledge support from MHRD, USIEF, India and IIE grant E0610103. This work benefited from discussions with Prof. M. Wallace, C. Jaliha, S. Paleri, P. Kushwah and Dr. J. Phadatare. We thank Prof. Christian Dominguez-Sarmiento and an anonymous reviewer for their useful comments. The rainfall data used in the study is obtained from the IMD ([http://imd pune.gov.in/ndc\\_new/Request.html](http://imd pune.gov.in/ndc_new/Request.html)). The global monsoon low pressure systems track dataset is available at <http://worldmonsoons.org/global-monsoon-disturbance-track-dataset/>. The ERA-interim dataset is available at <https://apps.ecmwf.int/datasets/data/interim-full-daily/>.

## References

- Adames, Á. F., & Ming, Y. (2018a). Interactions between water vapor and potential vorticity in synoptic-scale monsoonal disturbances: moisture vortex instability. *Journal of the Atmospheric Sciences*, 75(6), 2083–2106.
- Adames, Á. F., & Ming, Y. (2018b). Moisture and moist static energy budgets of south asian monsoon low pressure systems in gfdl am4. 0. *Journal of the Atmospheric Sciences*, 75(6), 2107–2123.
- Ajayamohan, R., Merryfield, W. J., & Kharin, V. V. (2010). Increasing trend of synoptic

- activity and its relationship with extreme rain events over central india. *Journal of Climate*, 23(4), 1004–1013.
- Baisya, H., & Pattnaik, S. (2019). Orographic effect and multiscale interactions during an extreme rainfall event. *Environmental Research Communications*, 1(5), 051002.
- Bartels, D. L., Brown, J. M., & Tollerud, E. I. (1997). Structure of a midtropospheric vortex induced by a mesoscale convective system. *Monthly weather review*, 125(2), 193–211.
- Bartels, D. L., & Maddox, R. A. (1991). Midlevel cyclonic vortices generated by mesoscale convective systems. *Monthly Weather Review*, 119(1), 104–118.
- Boos, W., Hurley, J., & Murthy, V. (2015). Adiabatic westward drift of indian monsoon depressions. *Quarterly Journal of the Royal Meteorological Society*, 141(689), 1035–1048.
- Bosart, L. F., & Sanders, F. (1981). The johnstown flood of july 1977: A long-lived convective system. *Journal of the Atmospheric Sciences*, 38(8), 1616–1642.
- Bretherton, C. S., Peters, M. E., & Back, L. E. (2004). Relationships between water vapor path and precipitation over the tropical oceans. *Journal of climate*, 17(7), 1517–1528.
- Carlowicz, M. (2019). *Heavy monsoon rains flood south asia*. Retrieved from <https://earthobservatory.nasa.gov/images/145460/heavy-monsoon-rains-flood-south-asia>
- Carr, F. H. (1977). Mid-tropospheric cyclones of the summer monsoon. *pure and applied geophysics*, 115(5-6), 1383–1412.
- Chakraborty, A. (2016). A synoptic-scale perspective of heavy rainfall over chennai in november 2015. *Current Science (00113891)*, 111(1).
- Coumou, D., & Rahmstorf, S. (2012). A decade of weather extremes. *Nature climate change*, 2(7), 491.
- Dash, S., Kumar, J. R., & Shekhar, M. (2004). On the decreasing frequency of monsoon depressions over the indian region. *Current Science*, 1404–1411.
- Dee, D. P., Uppala, S. M., Simmons, A. J., Berrisford, P., Poli, P., Kobayashi, S., ... Vitart, F. (2011, Apr). The ERA-Interim reanalysis: configuration and performance of the data assimilation system. *Quarterly Journal of the Royal Meteorological Society*, 137(656), 553–597.
- Doswell III, C. A., Brooks, H. E., & Maddox, R. A. (1996). Flash flood forecasting: An ingredients-based methodology. *Weather and Forecasting*, 11(4), 560–581.
- Emori, S., & Brown, S. (2005). Dynamic and thermodynamic changes in mean and extreme precipitation under changed climate. *Geophysical Research Letters*, 32(17).
- Falcão, A. X., Stolfi, J., & de Alencar Lotufo, R. (2004). The image foresting transform: Theory, algorithms, and applications. *IEEE transactions on pattern analysis and machine intelligence*, 26(1), 19–29.
- Findlater, J. (1969). A major low-level air current near the indian ocean during the northern summer. *Quarterly Journal of the Royal Meteorological Society*, 95(404), 362–380.
- Francis, P., & Gadgil, S. (2006). Intense rainfall events over the west coast of india. *Meteorology and Atmospheric Physics*, 94(1-4), 27–42.
- Fritsch, J., Murphy, J., & Kain, J. (1994). Warm core vortex amplification over land. *Journal of the atmospheric sciences*, 51(13), 1780–1807.
- George, P. (1956). Effect of off-shore vortices on rainfall along the west coast of india. *Indian J. Meteorol. Geophys*, 7, 225–240.
- Godbole, R. V. (1977). The composite structure of the monsoon depression. *Tellus*, 29(1), 25–40.
- Goswami, B., Ajayamohan, R., Xavier, P. K., & Sengupta, D. (2003). Clustering of synoptic activity by indian summer monsoon intraseasonal oscillations. *Geophysical Research Letters*, 30(8).
- Goswami, B. N., Venugopal, V., Sengupta, D., Madhusoodanan, M., & Xavier, P. K. (2006). Increasing trend of extreme rain events over India in a warming environment. *Science*, 314(5804), 1442–1445.
- Hodges, K. (1995). Feature tracking on the unit sphere. *Monthly Weather Review*, 123(12), 3458–3465.

- Hodges, K. (1999). Adaptive constraints for feature tracking. *Monthly Weather Review*, 127(6), 1362–1373.
- Holloway, C. E., & Neelin, J. D. (2009). Moisture vertical structure, column water vapor, and tropical deep convection. *Journal of the atmospheric sciences*, 66(6), 1665–1683.
- Houze Jr, R., McMurdie, L., Rasmussen, K., Kumar, A., & Chaplin, M. (2017). Multiscale aspects of the storm producing the june 2013 flooding in uttarakhand, india. *Monthly Weather Review*, 145(11), 4447–4466.
- Hunt, K. M., & Fletcher, J. K. (2019). The relationship between indian monsoon rainfall and low-pressure systems. *Climate Dynamics*, 1–13.
- Hurley, J. V., & Boos, W. R. (2015). A global climatology of monsoon low-pressure systems. *Quarterly Journal of the Royal Meteorological Society*, 141(689), 1049–1064.
- Joseph, P., & Sijikumar, S. (2004). Intraseasonal variability of the low-level jet stream of the asian summer monsoon. *Journal of Climate*, 17(7), 1449–1458.
- Karmakar, N., Chakraborty, A., & Nanjundiah, R. S. (2015). Decreasing intensity of monsoon low-frequency intraseasonal variability over india. *Environmental Research Letters*, 10(5), 054018.
- Karmakar, N., Chakraborty, A., & Nanjundiah, R. S. (2017). Increased sporadic extremes decrease the intraseasonal variability in the Indian summer monsoon rainfall. *Scientific reports*, 7(1), 7824.
- Knierel, J. C., & Johnson, R. H. (2002). The kinematics of a midlatitude, continental mesoscale convective system and its mesoscale vortex. *Monthly weather review*, 130(7), 1749–1770.
- Knierel, J. C., & Johnson, R. H. (2003). A scale-discriminating vorticity budget for a mesoscale vortex in a midlatitude, continental mesoscale convective system. *Journal of the atmospheric sciences*, 60(6), 781–794.
- Krishnamurthy, V., & Ajayamohan, R. (2010). Composite structure of monsoon low pressure systems and its relation to indian rainfall. *Journal of Climate*, 23(16), 4285–4305.
- Krishnamurti, T., & Hawkins, R. (1970). Mid-tropospheric cyclones of the southwest monsoon. *Journal of Applied Meteorology*, 9(3), 442–458.
- Krishnamurti, T., Kanamitsu, M., Godbole, R., Chang, C., Carr, F., & Chow, J. (1975). Study of a monsoon depression (i): Synoptic structure. *J. Meteor. Soc. Japan*, 53, 227–239.
- Kumar, A., Dudhia, J., Rotunno, R., Niyogi, D., & Mohanty, U. (2008). Analysis of the 26 july 2005 heavy rain event over mumbai, india using the weather research and forecasting (wrf) model. *Quarterly Journal of the Royal Meteorological Society*, 134(636), 1897–1910.
- Maddox, R. A., Chappell, C. F., & Hoxit, L. R. (1979). Synoptic and meso- $\alpha$  scale aspects of flash flood events. *Bulletin of the American Meteorological Society*, 60(2), 115–123.
- Maddox, R. A., Hoxit, L. R., Chappell, C. F., & Caracena, F. (1978). Comparison of meteorological aspects of the big thompson and rapid city flash floods. *Monthly Weather Review*, 106(3), 375–389.
- Miller, F. R., & Keshavamurthy, R. (1968). *Structure of an arabian sea summer monsoon system*. Univ of Hawaii Pr.
- Muller, C. J., O’Gorman, P. A., & Back, L. E. (2011). Intensification of precipitation extremes with warming in a cloud-resolving model. *Journal of Climate*, 24(11), 2784–2800.
- Murakami, T., Nakazawa, T., & He, J. (1984). On the 40-50 day oscillations during the 1979 northern hemisphere summer. *Journal of the Meteorological Society of Japan. Ser. II*, 62(3), 440–468.
- Nikumbh, A. C., Chakraborty, A., & Bhat, G. (2019). Recent spatial aggregation tendency of rainfall extremes over india. *Scientific reports*, 9(1), 10321.
- O’Gorman, P. A. (2015). Precipitation extremes under climate change. *Current climate change reports*, 1(2), 49–59.
- Phadtare, J. (2018). Role of eastern ghats orography and cold pool in an extreme rainfall event over chennai on 1 december 2015. *Monthly Weather Review*, 146(4), 943–965.

- Phadtare, J., & Bhat, G. (2019). Characteristics of deep cloud systems under weak and strong synoptic forcing during the indian summer monsoon season. *Monthly Weather Review*, *147*(10), 3741–3758.
- Pradhan, P., Dasamsetti, S., Ramakrishna, S., Dodla, V., & Panda, J. (2015). Mesoscale simulation of off-shore trough and mid-tropospheric cyclone associated with heavy rainfall along the west coast of india using armex reanalysis. *International Journal of Earth and Atmospheric Science*, *2*(1), 01–15.
- Rajeevan, M., Bhate, J., & Jaswal, A. K. (2008). Analysis of variability and trends of extreme rainfall events over india using 104 years of gridded daily rainfall data. *Geophysical Research Letters*, *35*(18), L18707.
- Rajeevan, M., Bhate, J., Kale, J., & Lal, B. (2006). High resolution daily gridded rainfall data for the indian region: Analysis of break and active. *Current Science*, *91*(3), 296–306.
- Rao, K., & Rajamani, S. (1970). Diagnostic study of a monsoon depression by geostrophic baroclinic model. *Indian Journal of Meteorology and Geophysics*, *21*, 187–194.
- Rao, Y. (1976). Southwest monsoon. *Meteorological monograph synoptic meteorology*, *1*, 2.2.
- Rasmussen, K. L., & Houze Jr, R. A. (2012). A flash-flooding storm at the steep edge of high terrain: disaster in the himalayas. *Bulletin of the American Meteorological Society*, *93*(11), 1713–1724.
- Raymond, D., & Jiang, H. (1990). A theory for long-lived mesoscale convective systems. *Journal of the atmospheric sciences*, *47*(24), 3067–3077.
- Sanders, F. (1984). Quasi-geostrophic diagnosis of the monsoon depression of 5–8 july 1979. *Journal of the Atmospheric Sciences*, *41*(4), 538–552.
- Schumacher, R. S., & Johnson, R. H. (2005). Organization and environmental properties of extreme-rain-producing mesoscale convective systems. *Monthly weather review*, *133*(4), 961–976.
- Schumacher, R. S., & Johnson, R. H. (2009). Quasi-stationary, extreme-rain-producing convective systems associated with midlevel cyclonic circulations. *Weather and Forecasting*, *24*(2), 555–574.
- Sikka, D. (1977). Some aspects of the life history, structure and movement of monsoon depressions. *pure and applied geophysics*, *115*(5), 1501–1529.
- Sikka, D. (1978). Some aspects of the life history, structure and movement of monsoon depressions. In *Monsoon dynamics* (pp. 1501–1529). Springer.
- Sutcliffe, R. (1947). A contribution to the problem of development. *Quarterly Journal of the Royal Meteorological Society*, *73*(317-318), 370–383.
- Thiruppugazh, V. (2019). *Gujarat flood 2017 case study*. Retrieved from <https://ndma.gov.in/images/guidelines/gujrat-flood-study-2017.pdf>
- Trenberth, K. E. (1978). On the interpretation of the diagnostic quasi-geostrophic omega equation. *Monthly Weather Review*, *106*(1), 131–137.
- Trenberth, K. E. (1999, May 01). Conceptual framework for changes of extremes of the hydrological cycle with climate change. *Climatic Change*, *42*(1), 327–339.
- Vishnu, S., Francis, P., Shenoi, S., & Ramakrishna, S. (2016). On the decreasing trend of the number of monsoon depressions in the bay of bengal. *Environmental Research Letters*, *11*(1), 014011.
- Wang, B. (2006). *The asian monsoon*. Springer Science & Business Media.

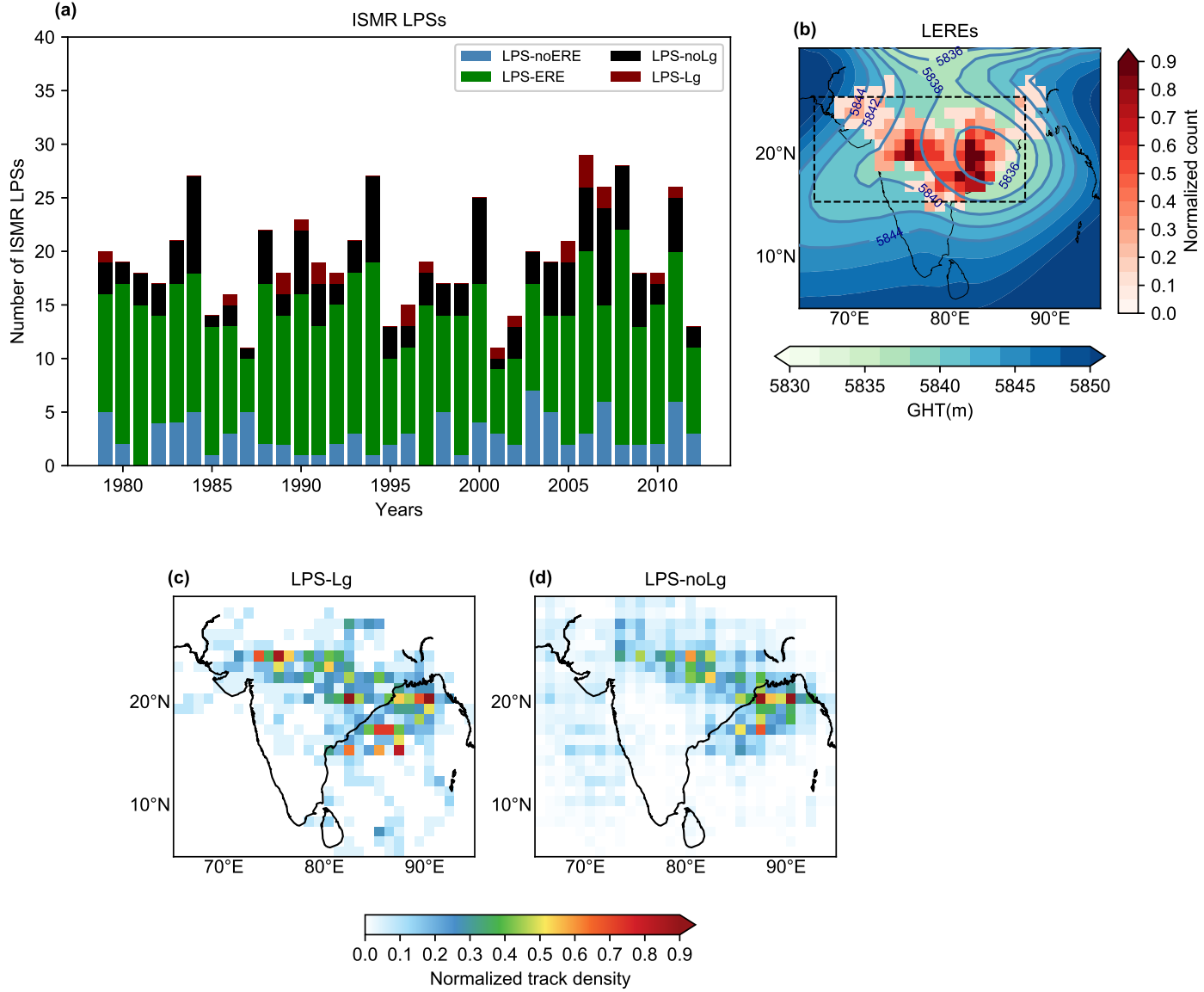


**Figure 1.** (a) Seasonal counts of monsoon low pressure systems (LPSs) that lead to extreme rainfall events (LPS-ERE), LPSs that did not lead to an ERE (LPS-noERE), LPSs that lead to LEREs (LPS-Lg), strong LPSs (intensity  $\geq 2$ ) that did not cause LEREs (LPS-noLg) observed during the study period (1979-2012). (b) Spatial distribution of LEREs and the JJAS climatology of geopotential height at 500 hPa. The count of LEREs is normalized by the maximum count over the study region ( $15^{\circ} - 25^{\circ}\text{N}$ ,  $65^{\circ} - 85^{\circ}\text{E}$ ). Track density of (c) LPS-Lg and (d) LPS-noLg. The track density is the number of tracks of LPSs per grid and is normalized with respect to the maximum value over the region ( $0^{\circ} - 30^{\circ}\text{N}$ ,  $60^{\circ} - 90^{\circ}\text{E}$ ). The dotted inset box in Fig 1b. represents the study region ( $15^{\circ} - 25^{\circ}\text{N}$ ,  $65^{\circ} - 85^{\circ}\text{E}$ ).

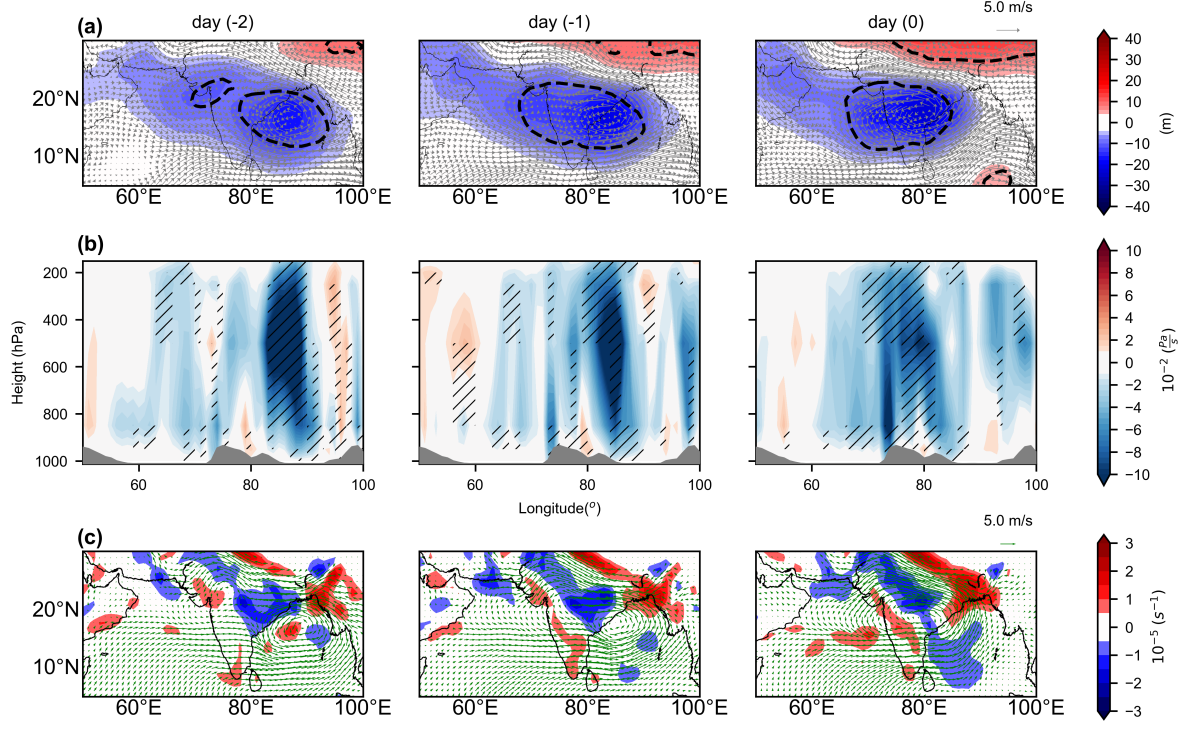


**Figure 2.** Lagged composites of anomalous (a) geopotential height ( $m$ ), wind ( $\frac{m}{s}$ ) at 500 hPa, (b) pressure velocity ( $\frac{Pa}{s}$ ), and (c) wind divergence ( $s^{-1}$ ), wind ( $\frac{m}{s}$ ) at 850 hPa for LPS-Lg from day(-2) to day(0) (left to right). Day-0 indicates the day of LERE. The pressure velocity is meridionally averaged from 15° to 25°N. The dotted contour and hatching represent statistically significant anomalies for geopotential height (t-test:  $p-value < 0.01$ ) and pressure velocity (t-test:  $p-value < 0.05$ ), respectively.

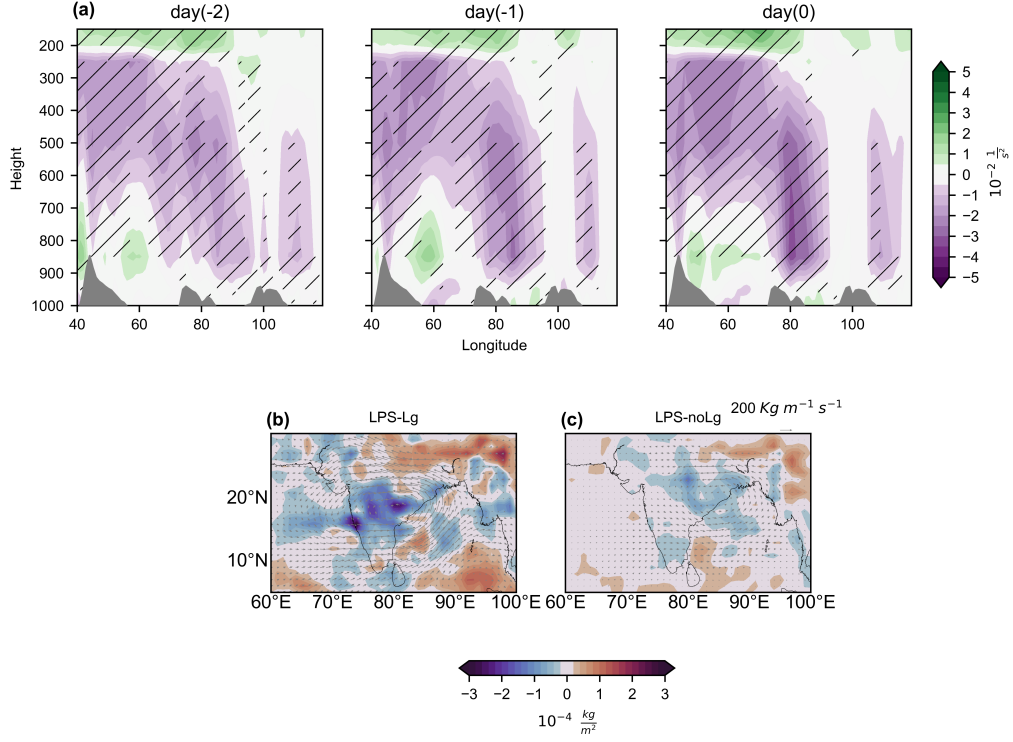


**Figure 3.** (a) Lagged composite of static stability anomalies for LPS-Lg from lag day(-2) to day(0). The anomalies are meridionally averaged from 15° to 25°N. The hatching represents statistically significant anomalies (t-test:  $p$  - value < 0.05). Composite vertically integrated moisture divergence (shading) and moisture transport (vectors) anomalies for (b)LPS-Lg on the LERE day and for (c)LPS-noLg at the middle location of the LPS track.

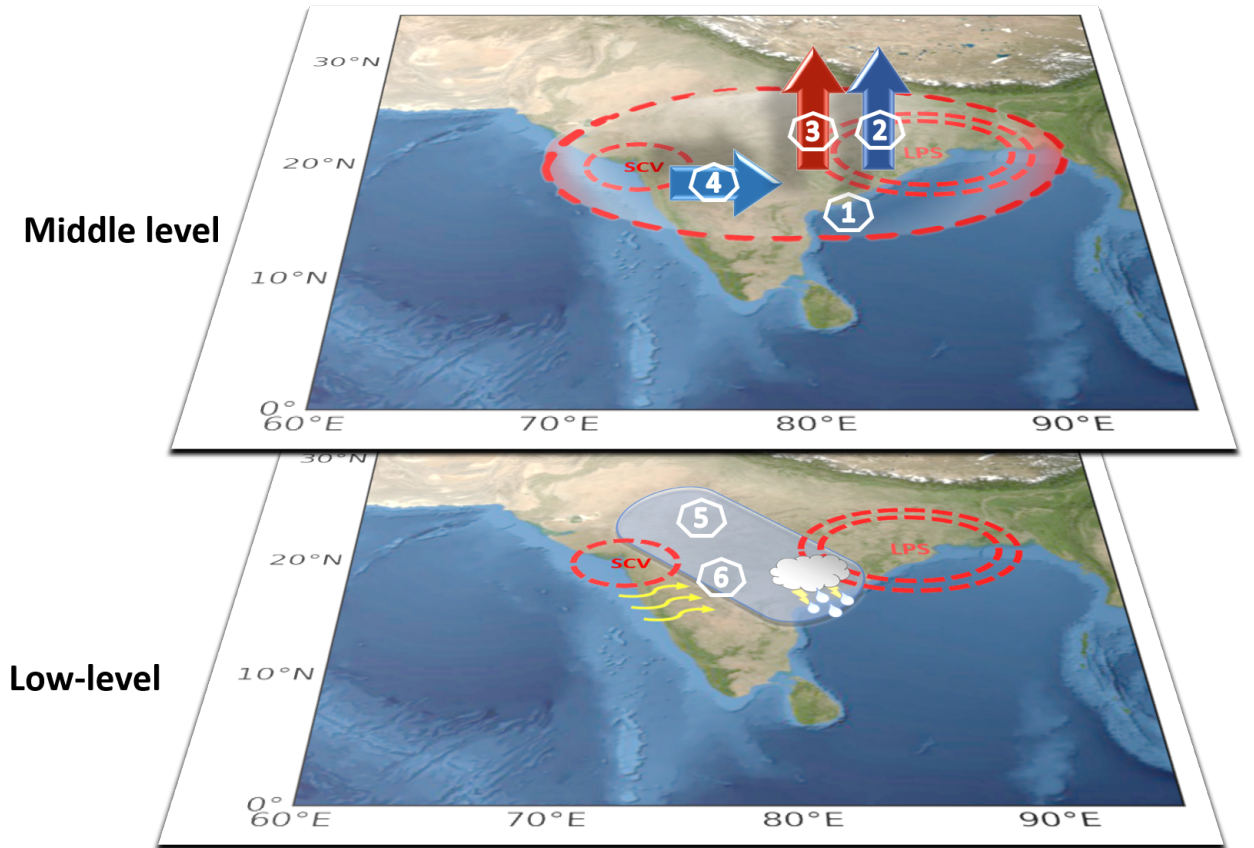


**Figure 4.** Schematic explaining the mechanism of LEREs. The interaction of an LPS and an SCV forms conditions favourable for long-lived, organized and slow moving convective systems on the western flank of the LPS, which result in LEREs. The numbers from 1 to 6 in the figure are representative of terms viz., mid-tropospheric vortex, dynamic lifting, static instability, moisture supply, an organization at the low-level, and LPS translation speed, respectively. These terms are explained in the summary section.

Figure 1.

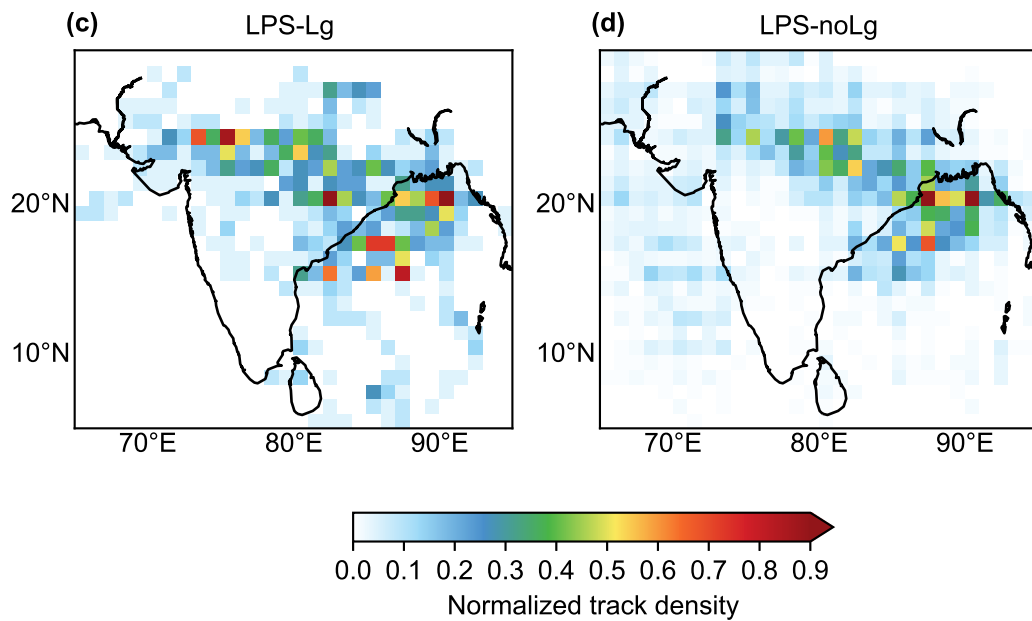
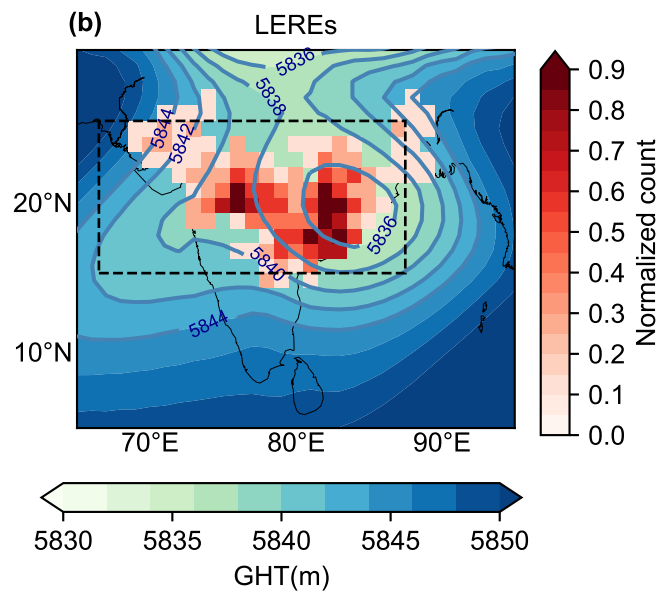
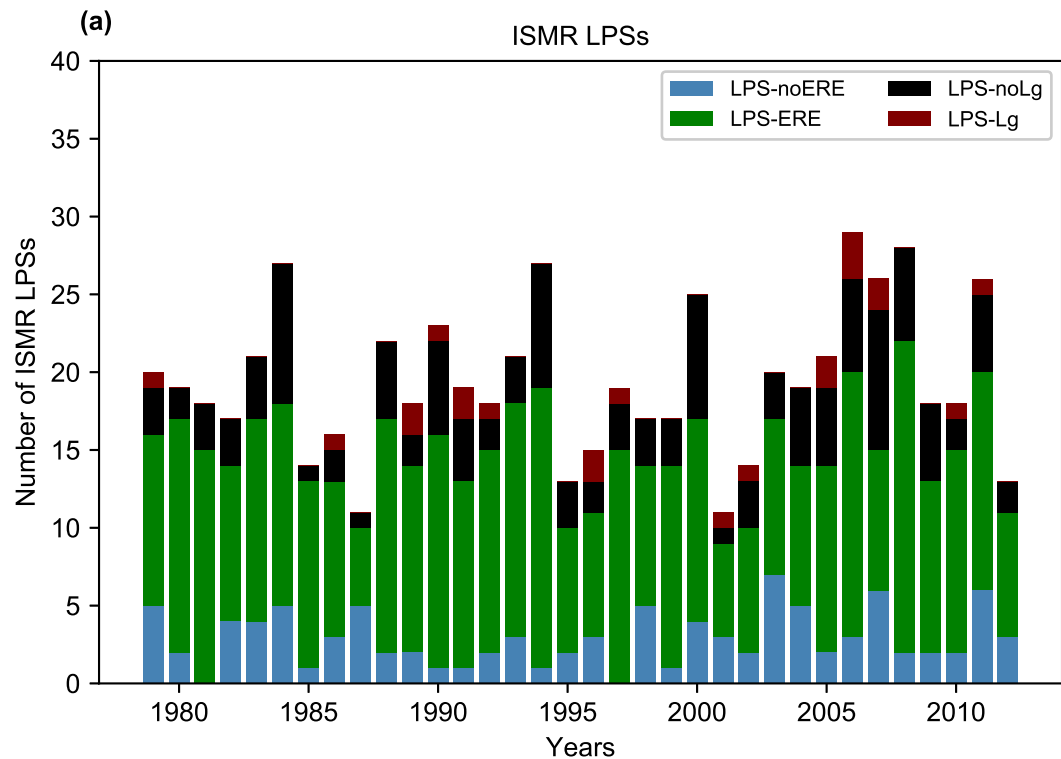


Figure 2.

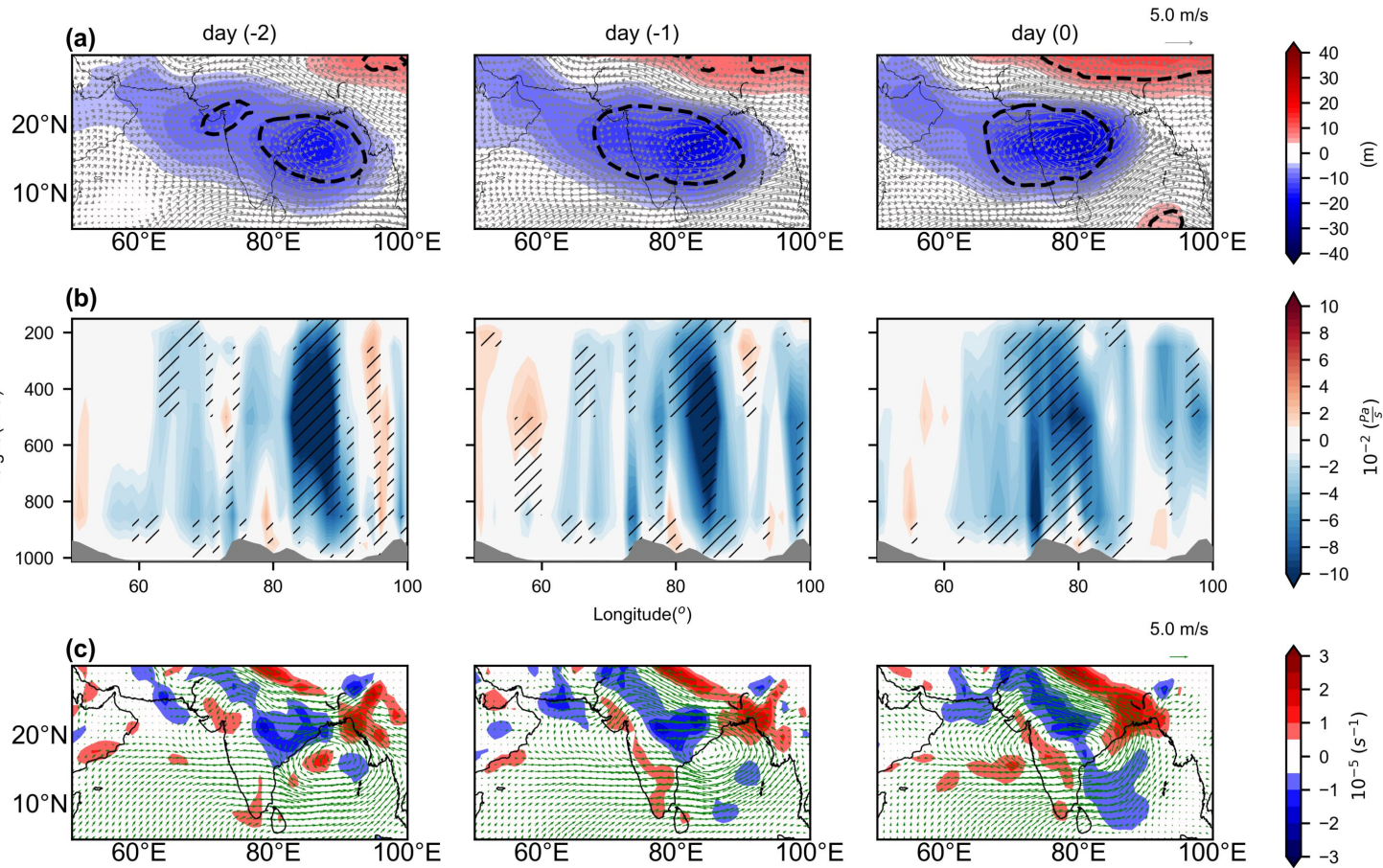


Figure 3.

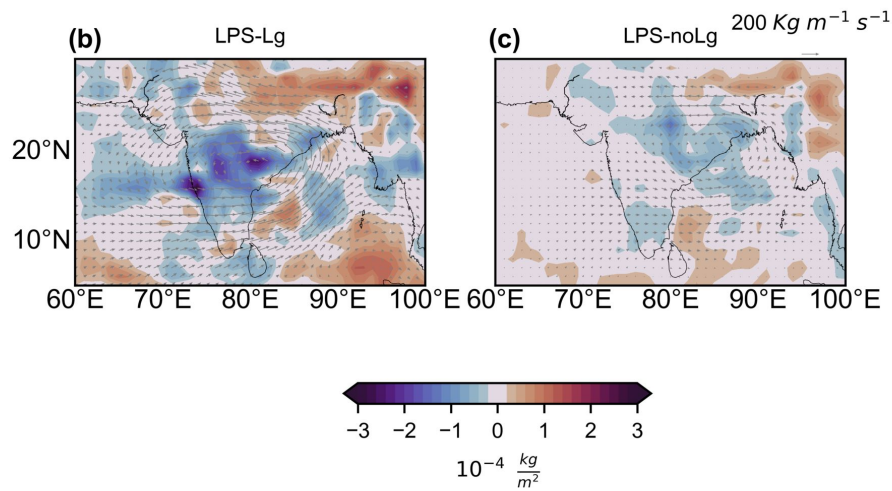
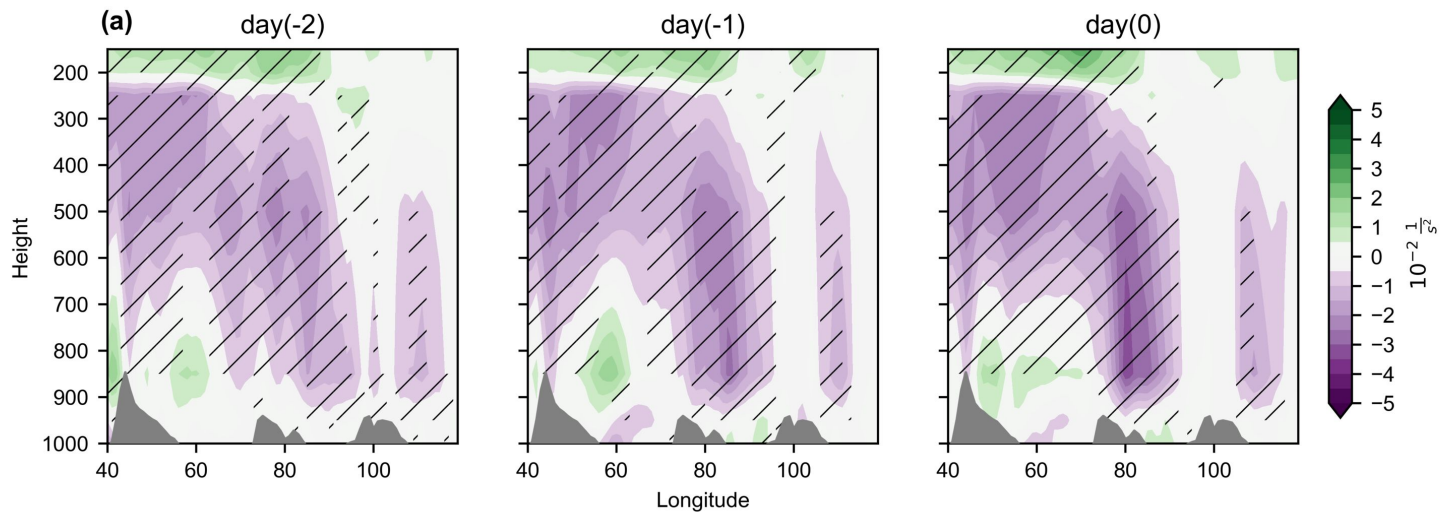
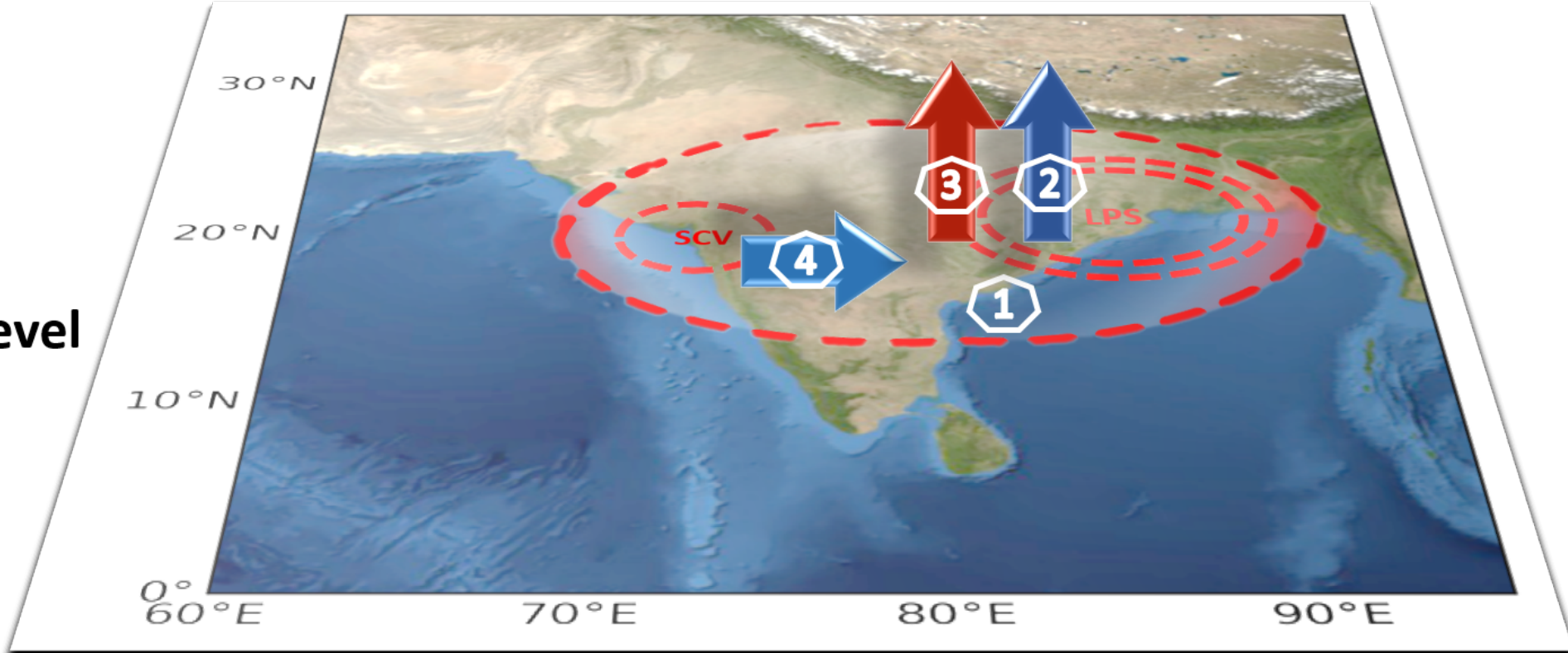


Figure 4.

Middle level



Low-level

